J Fluoresc (2017) 27:1307–1321
DOI 10.1007/s10895-017-2065-7

ORIGINAL ARTICLE

Coumarin Based Fluorescent Probe for Colorimetric Detection of Fe^{3+} and Fluorescence Turn On-Off Response of Zn^{2+} and Cu^{2+}

Nayan Roy[1] · **Abhijit Dutta**[1] · **Paritosh Mondal**[1] · **Pradip C. Paul**[1] · **T. Sanjoy Singh**[1]

Received: 10 November 2016 / Accepted: 2 March 2017 / Published online: 15 March 2017

Abstract A new coumarin based Schiff-base chemosensor-(E)-7-(((8-hydroxyquinolin-2-yl)methylene) amino)-4-methyl-2H-chromen-2-one (**$H_{11}L$**) was synthesized and evaluated as a colorimetric sensor for Fe^{3+} and fluorescence "turn on-off" response of Zn^{2+} and Cu^{2+} using absorption and fluorescence spectroscopy. Upon treatment with Fe^{3+} and Zn^{2+}, the absorption intensity as well as the fluorescence emission intensity increases drastically compared to other common alkali, alkaline earth and transition metal ions, with a distinct color change which provide naked eye detection. Formation of 1:1 metal to ligand complex has been evaluated using Benesi-Hildebrand relation, Job's plot analyses, ^{1}H NMR titration as well as ESI-Mass spectral analysis. The complex solution of **$H_{11}L$** with Zn^{2+} ion exhibited reversibility with EDTA and regenerate free ligand for further Zn^{2+} sensing. **$H_{11}L$** exhibits two INHIBIT logic gates with two different chemical inputs (i) Zn^{2+} (IN1) and Cu^{2+} (IN2) and (ii) Zn^{2+} (IN1) and EDTA (IN2) and the emission as output. Again, an IMPLICATION logic gate is obtained with Cu^{2+} and EDTA as chemical inputs and emission as output mode. Both free ligand as well as metal-complexes was optimized using density functional theory to interpret spectral properties. The corresponding energy difference between HOMO-LUMO energy gap for **$H_{11}L$**, $H_{11}L$-Zn^{2+} and $H_{11}L$-Cu^{2+} are 2.193, 1.834 and 0.172 eV, respectively.

Keywords Chemosensor · Fluorescence · Selectivity · Binding constant · Logic function · Density functional theory

✉ T. Sanjoy Singh
takhelsingh@gmail.com; singhsanjoy2002@yahoo.co.in

[1] Department of Chemistry, Assam University, Silchar, Assam 788 011, India

Introduction

Development of fluorescent chemosensor for sensing of biologically and environmentally important metal ions has been receiving considerable attention in the field of chemical sensors [1, 2]. They are usually very sensitive, low cost, easily performed and versatile, which are also used for real-time monitoring and detection of metal ions at a molecular level and are applicable in many fields such as medical diagnostics, environmental control, living cells and electronics. Nowadays, among the different analyte, special interest is devoted to develop chemosensors for transition metal ions, usually they represent an environmental concern when present in uncontrolled amounts, but at the same time some of them such as iron, zinc, manganese, copper and cobalt are present as essential elements in biological systems. Among biologically important metal ions, iron, copper and zinc ion are the most three abundant and essential trace elements in the human body which play important roles in biology, chemistry and environment. Iron is the most abundant transition metal ion present in the human body. Fe^{3+} ion is an important and essential for proper functioning of all living cells and acts as a cofactor in many enzymatic reactions to human as well as in specialized transport and storage of proteins [3]. The deficiency of Fe^{3+} causes anaemia, liver damage, diabetes, hemochromatosis, Parkinson's disease and cancer [4]. On the other side, zinc is the second most abundant transition metal ion in the human body after iron, and plays a myriad of roles in numerous cellular functions such as regulation of gene expression, apoptosis, co-factors in metalloenzyme catalysis and neurotransmission in biological systems [5, 6]. Many severe neurological diseases, including Alzheimer's disease, cerebral ischemia and epilepsy [7–9] are associated with the disorder of Zn^{2+} metabolism. Therefore, estimation of Zn^{2+} is very important in neurobiology. However, if unregulated, Fe^{3+} and Zn^{2+} may cause many

severe diseases, such as β-thalassemia, Friedreich's ataxia, Alzheimer's disease, Parkinson's disease and epilepsy [10]. Therefore, there is a great need for developing Zn^{2+} and Fe^{3+} selective sensors that can distinguish Zn^{2+} and Fe^{3+} from other transition metal ions. Many sensors reports are available for detection of both Fe and Zn with synthetic difficulties which require laborious multistep organic synthesis. However, despite much attention of fluorescent sensors for selective and sensitive detection of both Fe^{3+} and Zn^{2+}, there is still a huge demand for new sensors with improved properties, low-cost, requirement of less labour and efficient sensors. At the same time, copper is the third most abundant trace element in the human body as well as in many living organisms. Copper plays a vital part in the physiological processes of organisms, including connective tissue development and the formation of bone and blood. However, any alternation in the uptake of copper may lead to neurodegenerative disorders such as Menkes and Wilson diseases [11–13], familial amyotropic lateral sclerosis [14, 15] and Prion diseases [16]. Thus the development of chemosensors for selective and sensitive detection of these trace elements like Fe^{3+}, Cu^{2+} and Zn^{2+}, still remains a challenge and active field of research.

Research on molecular logic gates has focused mainly in the field of chemistry research for its application in information technology since the first AND logic gate was mimicked with optical signals [17]. Various chemical systems have been developed to exhibit different operations like AND, OR, NOT and their integrated operations [18]. In addition, many useful integrated logic gates such as INHIBIT, half subtractor, half adder, full adder, and full subtractor with various single molecules have been exploited [19, 20]. However, during literature surveys, very few IMPLICATION logic gate are reported so far [21]. Recently, there has been reported several molecular logic gates based on the structure of salicylidine Schiff base [22–25]. Some of the coumarin Schiff base was also reported as molecular switch for dual sensing of different metal ions [26, 27].

The nitrogen atom of azomethine C = N double bond in Schiff base also exhibits a strong affinity for transition metal ions. Therefore, the Schiff base are known to be good ligand for metal ions and used to develop chemosensors. In addition, Schiff base derivatives incorporating a fluorescent moiety are appealing tools for optical sensing of metal ions. Nowadays, designing and synthesis of fluorescent sensors with high selectivity and sensitivity to metal ions is an important and vibrant field. Many excellent metal ions sensors have been contributed significantly but some of the reported synthesis methods are always too complicated. However, only a few coumarin based chemosensors are reported so far for the dual sensing of metal ions [28–34]. As it is well known that coumarin framework exhibits various interesting photophysical properties such as large Stokes shift with visible excitation and emission wavelengths, high quantum yields, good photostability and also has wide application as fluorescent dyes [35–37]. Moreover in the literature, only few coumarin based Schiff base were reported and known to selectively recognize for dual sensing of metal ions [26, 27, 38, 39]. So, in this paper, we have designed and synthesized a new coumarin based Schiff-base fluorescent probe-(E)-7-(((8-hydroxyquinolin-2-yl)methylene)amino)-4-methyl-2H-chromen-2-one ($\mathbf{H_{11}L}$) by one step condensation of 7-Amino-4-methyl coumarin and 8-hydroxy quinoline 2-carbaldehyde in methanol solution (Scheme 1) which was selectively and sensitively recognized both Zn^{2+} and Cu^{2+} using fluorescence spectroscopy. Herein, the photophysical properties of $\mathbf{H_{11}L}$ were studied in presence of different metal ions, focusing the attention on their absorption and emission properties using absorption and fluorescence spectroscopy. In the UV-Vis absorption studies, a strong absorption band at 240 nm, 265 nm, 290 nm and 355 nm were observed in ethanol solution. On addition of Fe^{3+}, the absorption intensity was found to increase with a dramatic change in color which can be easily detected with naked eye. This clearly indicates that $\mathbf{H_{11}L}$ is a highly selective colorimetric sensor for Fe^{3+} compared to other survey metal ions. It was also seen that the absorption peak at 355 nm disappeared and a new absorption peak at 335 nm appeared with gradual addition of Fe^{3+} ion. At the same time, we also observed an isosbestic point at 360 nm which clearly indicates complex formation due to metal ion binding. We also observed a pronounced fluorescence enhancement in presence of Zn^{2+}, while there was no change or minimal spectral changes in presence of other metal ions except Cu^{2+} which shows fluorescence quenching. This chemosensor was used as a fluorescent "turn on-off" detector of Zn^{2+} and Cu^{2+} ion, respectively. Importantly, it was able to distinguish Zn^{2+} from Cd^{2+} besides having very similar chemical properties often respond together with similar spectral changes. Moreover, the fluorescence emission behavior of $\mathbf{H_{11}L}$ can be utilized to study as a binary logic function comprising of two INHIBIT logic gates with two different chemical inputs (i) Zn^{2+} (IN1) and Cu^{2+} (IN2) and (ii) Zn^{2+} (IN1) and EDTA (IN2) and the emission as output. Again, an IMPLICATION logic gate is obtained with Cu^{2+} and EDTA as chemical inputs and emission as output mode. Structure of $\mathbf{H_{11}L}$ and its metal complexes were fully optimized using BLYP functional and DNP basis sets as implemented in the program $DMol^3$. The corresponding energy difference between HOMO-LUMO energy gap for $\mathbf{H_{11}L}$, $H_{11}L$-Zn^{2+} and $H_{11}L$-Cu^{2+} are 2.193, 1.834 and 0.172 eV, respectively. Chemical hardness for both ligand as well as its metal complexes was also calculated.

Experimental Details

Materials

8-hydroxy quinoline 2-carbaldehyde and 7-Amino-4-methyl coumarin was obtained from Sigma-Aldrich Chemical

Scheme 1 Reaction scheme for the synthesis of (E)-7-(((−hydroxyquinoline-2-yl)methylene)amine)-4-methyl-2H-chromen-2-one (**$H_{11}L$**)

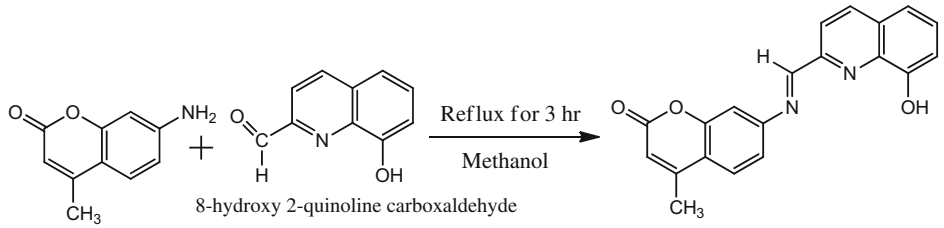

Company. All the spectroscopic grade solvents used were obtained from Sisco Research Laboratory (SRL) Pvt. Ltd. and in some cases, from Aldrich Chemical Company. Chemical reagents were obtained from Lancaster as well as S.D. Fine Chemical Ltd. All experiments were carried out at room temperature.

Synthesis and Characterization of $H_{11}L$

A portion of the 8-hydroxy quinoline 2-carbaldehyde (0.173 g, 1 mmol) and 7-Amino-4-methyl) coumarin (0.175 g, 1 mmol) was separately dissolved in absolute ethanol and were combined together to get to yellow color. The solution was stirred under reflux conditions for 3 h in presence of 2–3 drops of acetic acid and precipitate was filtrated, washed with cold absolute ethanol three times, then recrystallized with ethanol/chloroform (1/3, *v*/v) to get deep yellow microcrystal (**$H_{11}L$**) in 80% yield. m.p. 151 °C. IR (max, cm^{-1}, KBr): 3435(ν_{OH}), 3192(ν_{as}(C-H), 2987(ν_s(C-H),), 1629(ν(C = N)), 1575(C = C), 1236(ν(C-O)), 1120(ν(CN)),784(ν(C-H)); ^{1}H NMR (400 MHz, $CDCl_3$, TMS, δ, ppm): 10.16 (s, H-1), 7.21 (d, H-2), 7.59 (t, H-3), 7.64 (d, H-4), 8.59 (d, H-5),7.84 (d, H-6), 8.27 (s, H-7), 7.07(s, H-8), 7.29 (d, H-9), 7.74 (d, H-10), 2.42 (s, H-11), 6.18 (s, H-12); ^{13}C NMR (400 MHz, $CDCl_3$, TMS, δ, ppm):112.2, 112.5, 115.5, 117.9, 118.1, 119.0, 119.4, 120.1, 126.9, 128.1, 131.9, 136.1, 137.5, 148.6, 149.6, 151.4, 151.7, 152.7, 153.2, 160.8; Anal. Calc. for $C_{20}H_{14}N_2O_3$ (330.3): C, 72.72%; H, 4.27%; N, 8.48%. Found: C, 72.20%; H, 4.24%; N, 8.40%. ESI-MS, *m/z*: Calcd. for $C_{20}H_{14}N_2O_3$ $(M + H)^+$: 331.3, found: 331.5.

Physical Measurements

The IR spectra were measured on a PerkinElmer L 120000A spectrometer with KBr pellets in the range 4000–400 cm^{-1}. ^{1}H and ^{13}C NMR spectra were recorded on Bruker DPX-400 MHz spectrometer with chemical shifts reported as ppm (in $CDCl_3$, tetramethylsilane as internal standard). Elemental analyses were carried out using PE2400 elemental analyzer. pH measurement was recorded on Global Digital pH meter (DPH-500). Absorption and fluorescence emission spectra were recorded on a Shimadzu UV-1601PC absorption spectrophotometer and PerkinElmer LS 45 spectrofluorimeter, respectively. Fluorescence quantum yields (ϕ_f) were calculated by comparing the total fluorescence intensity under the whole fluorescence spectral range with that of a standard ($\phi_f = 0.546$, quinine sulfate in 1 M sulfuric acid) using the following equation as described before [40].

$$\varphi_f^i = \varphi_f^s \cdot \frac{F^i}{F^s} \cdot \frac{1-10^{-A^s}}{1-10^{-A^i}} \cdot \left(\frac{\eta^i}{\eta^s}\right)^2 \quad (1)$$

where F is the total fluorescence intensity under whole fluorescence spectral curve, A^i and A^s is the optical density of the sample and standard, respectively and η^i is the refractive index of the solvent at 298 K. Fluorescence lifetimes were recorded in a nano-LED based time-resolved fluorimeter obtained from Photo Technology International (PTI) using TCSPC technique. The instrument response function (IRF) was obtained at 360 nm using a dilute colloidal suspension of dried non-dairy coffee whitener. The half width of the IRF was ~100 ps. The samples were excited at 360 nm and the fluorescence emission was collected at corresponding emission wavelength. The number of counts in the peak channel was at least 10,000. In fluorescence lifetime measurements, the emission was monitored at the magic angle (54.7°) to eliminate the contribution from the decay of anisotropy.

Computational Methods

Quantum chemical calculations based on density functional theory (DFT) were carried out to investigate the electronic structure of **$H_{11}L$**, $H_{11}L$-Zn^{2+} and $H_{11}L$-Cu^{2+} complexes. Full geometry optimization of **$H_{11}L$**, $H_{11}L$-Zn^{2+} and $H_{11}L$-Cu^{2+} complexes has been carried out without imposing any constrain using BLYP functional [41, 42] which incorporates Becke's exchange and Lee-Yang-Parr correlation and double-numerical polarized (DNP) [43] basis sets as implemented in $DMol^3$ program package [44] using Kohn-Sham Theory [45, 46]. In order to confirm the stability of **$H_{11}L$**, $H_{11}L$-Zn^{2+} and $H_{11}L$-Cu^{2+} complexes, we performed vibrational frequency calculations at the same level of theory.

Results and Discussion

UV-Vis Titration Studies of $H_{11}L$

The absorption spectrum of **$H_{11}L$** shows four different peak positions at 245 nm, 260 nm, 290 nm and 355 nm respectively, in ethanol solution. The stock solution of the ligand and metal ions were prepared in 10 mM concentration in ethanol solution at room temperature. However, the experimental solution of free ligand (**$H_{11}L$**) was kept to be 2.5×10^{-4} M in all cases. In the absorption spectra, there are no remarkable changes in presence of other different metal ions like alkali (Na^+, K^+), alkaline earth (Ca^{2+}, Mg^{2+}, Sr^{2+}) and transition metal ions (Cd^{2+}, Ni^{2+}, Co^{2+}, Cu^{2+}, Zn^{2+}) except Fe^{3+}. To further investigate the interaction between **$H_{11}L$** and Fe^{3+}, UV-Vis absorption spectral variation of **$H_{11}L$** was monitored in presence of different concentration of Fe^{3+} in ethanol solution at room temperature. As shown in Fig. 1, gradual addition of Fe^{3+} (0-55 μM) resulted in an obvious change in absorption intensity as well as in color, from colorless to deep yellow, which can be easily detected with naked eye. This clearly indicates that **$H_{11}L$** is a highly selective colorimetric sensor for Fe^{3+} ions. It was also seen that the absorption peak at 355 nm disappeared and a new absorption peak at 335 nm appeared with gradual addition of Fe^{3+} (fig. 1). At the same time, we also observed an isosbestic point at 360 nm which clearly indicates complex formation due to metal ion binding. Here in presence of Fe^{3+}, an isomerization happened to **$H_{11}L$** due to intramolecular charge transfer (ICT) from O-H and N = CH which leads to imine bond breaking. Therefore, **$H_{11}L$** showed selective estimation for Fe^{3+} ions in UV-Vis absorption studies.

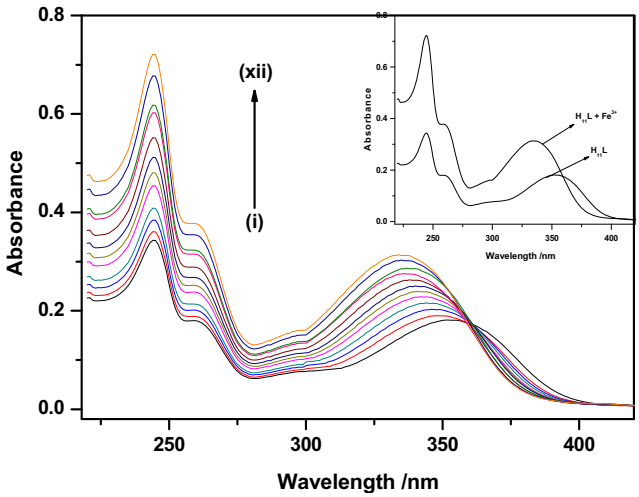

Fig. 1 Change in UV-Vis spectrum of **$H_{11}L$** (2.5×10^{-4} M) upon gradual addition of Fe^{3+} in ethanol solution at room temperature. The concentrations of Fe^{3+} (μM) are: 0.0 (i), 5.0 (ii), 10.0 (iii), 15.0 (iv), 20.0 (v), 25.0 (vi), 30.0 (vii), 35.0 (viii), 40.0 (ix), 45.0 (x), 50.0 (xi) and 55.0 (xii).Inset show the spectra of free ligand in absence (0 μM) and presence (55 μM) of Fe^{3+} ion concentration

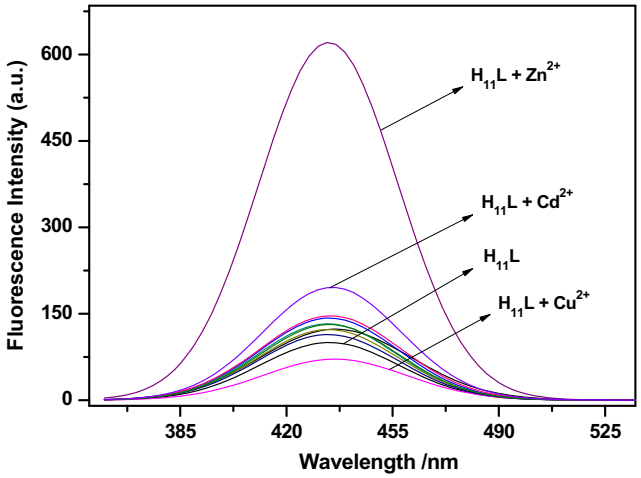

Fig. 2 Fluorescence emission spectra of **$H_{11}L$** (2.5×10^{-4} M) in absence and presence of different metal ions (~45 μM) at room temperature. Excitation was done at λ_{exc} = 355 nm

Fluorescence Studies of $H_{11}L$

In Presence of Different Metal Ion

The interactions of **$H_{11}L$** with different metal ions have been investigated by evaluating the changes in their fluorescence properties by addition of different metal ions in ethanol solution at room temperature. The fluorescence emission maxima peak of **$H_{11}L$** appeared at 438 nm upon excitation at 355 nm, which on addition of Zn^{2+} (~45 μM) gives slightly blue-shifted at 428 nm. However, the fluorescence emission intensity has been drastically increased with almost 6-fold (Fig. 2) in presence of Zn^{2+} (~45 μM). Similarly, in presence of other different metal ions like Na^+, K^+, Ca^{2+}, Mg^{2+} Cd^{2+}, Ni^{2+}, Co^{2+}, Ba^{2+}, Al^{3+}, Hg^{2+}, Mn^{2+} and Fe^{3+}, **$H_{11}L$** showed either no change in the fluorescence peak position or a very negligible amount of changes occurs in the fluorescence intensity in case of Cd^{2+}. So, there was no appreciable change in the fluorescence emission behavior of **$H_{11}L$** with others metal ions except for Zn^{2+}. However, in presence of Cu^{2+}, it also exhibits quenching of fluorescence emission intensity without any interference of other metal ions present in the solution. Fluorescence intensity profile changes of **$H_{11}L$** in presence of different metal ions were shown in the histogram (Fig. 3) which clearly indicates high selectivity of Zn^{2+}.Therefore, **$H_{11}L$** shows selective estimation for Zn^{2+} and Cu^{2+} ions in fluorescence studies.

Influence of Zn^{2+} Ion

As shown in Fig. 4, with gradual addition of Zn^{2+} (0–60 μM), a significant enhancement of the emission band intensity at 428 nm occurred, which resulted in a ~ 10 nm blue-shifted and a large increase in the fluorescence intensity. This effect was not observed in presence of other metal ions even with very

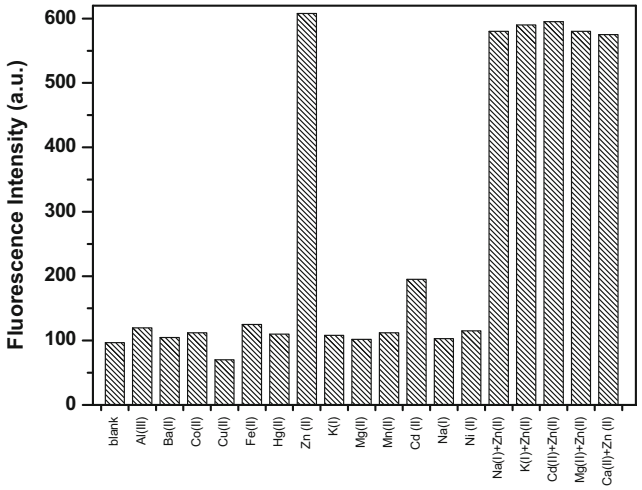

Fig. 3 Fluorescence intensity profile changes of $\mathbf{H_{11}L}$ in absence (free ligand) and presence of 45 μM concentration of various metal ions at room temperature. Fluorescence intensity changes that occur upon subsequent addition of Zn^{2+} ion (45 μM) in presence of different metal ions were also reported. Excitation was done at λ_{exc} = 355 nm

high concentration (say ~ 100 μM). The enhancement of fluorescence intensity was attributed to the introduction of Zn^{2+} and consequently occurrence of the strong complexation with $\mathbf{H_{11}L}$ via O-H and N heteroatoms which can be explain due to prevention of isomerization by metal ion binding. This coordination can enhance the planarity and rigidity which can also decrease nonradiative decay of the excited state and increased radiative decay which may be explained due to photoinduced electron transfer (PET) process between $\mathbf{H_{11}L}$ and Zn^{2+} [47–50].The fluorescence quantum yields were also calculated both in free ligand as well as in presence of Zn^{2+}. Here, the fluorescence quantum yield increases drastically from 0.6×10^{-3} for $\mathbf{H_{11}L}$ compared to 7.4×10^{-2} for $H_{11}L$-Zn^{2+} complex. Further, tolerance of fluorescence intensity due to Zn^{2+} (45 μM) in presence of 50 times an excess of other metal ions like Na^+, K^+, Cd^{2+}, Ca^{2+} and Mg^{2+} has been successfully verified as shown in Fig. 3. So, all competitive metal ions had no obvious interference with the detection of Zn^{2+}, which also indicates that $H_{11}L$-Zn^{2+} system was hardly affected by these coexistent metal ions. Thus, $\mathbf{H_{11}L}$ can be used as selective fluorescent chemosensor for Zn^{2+} determination in presence of other competing metal ions. The emission intensity of $\mathbf{H_{11}L}$ was linearly proportional to Zn^{2+} ion concentration. This linear dependence of Zn^{2+} ion concentration suggests that $\mathbf{H_{11}L}$ could be utilized for the quantitative estimation of Zn^{2+}. The detection limit was calculated using 3*S/M [51] where S is the standard deviation of a blank signal and M is the slope of the regression line. The detection limit was found to be in order of 10^{-6} M. Hence, $\mathbf{H_{11}L}$ shows selective estimation for Zn^{2+} and "turn-on" fluorescent sensor in presence of Zn^{2+} ion.

Influence of Cu^{2+} Ion

As it is well known, Cu^{2+} is a paramagnetic ion with an empty d-shell and can strongly quench the emission of a fluorophore via a photoinduced metal-to-fluorophore, electron or energy transfer mechanism [52, 53]. In addition, among the relevant paramagnetic metal ions, Cu^{2+} has a particularly high thermodynamic affinity for ligands with "N" or "O" as chelating element and fast metal-to-ligand binding kinetics process [54]. So, in order to evaluate the binding nature between $\mathbf{H_{11}L}$ and Cu^{2+}, a fluorescence titration with increasing concentration of Cu^{2+} (0-32 μM) was performed and a significant fluorescence emission intensity decrease with slight red-shifted (Fig. 5). This also clearly indicates complex formation

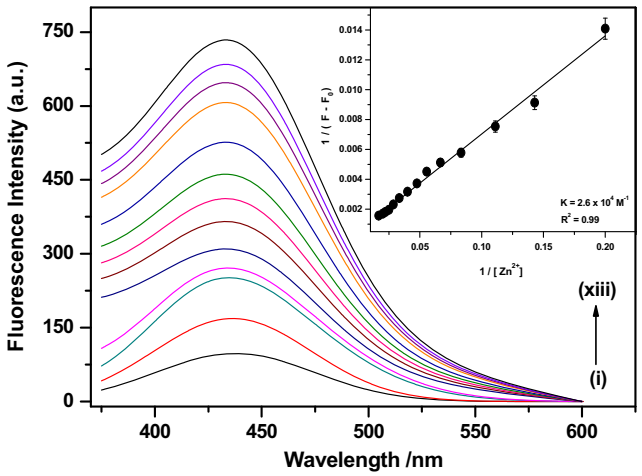

Fig. 4 Variation of fluorescence intensity of $\mathbf{H_{11}L}$ against concentration of Zn^{2+}. The concentrations of Zn^{2+} (μM) are: 0.0 (i), 5.0 (ii), 10.0 (iii), 15.0 (iv), 20.0 (v), 25.0 (vi), 30.0 (vii), 35.0 (viii), 40.0 (ix), 45.0 (x), 50.0 (xi), 55.0 (xii) and 60.0 (xiii). Inset show the double reciprocal plot of $1/(F\text{-}F_0)$ against $1/[Zn^{2+}]$ giving a straight line indicating 1:1 complex formation

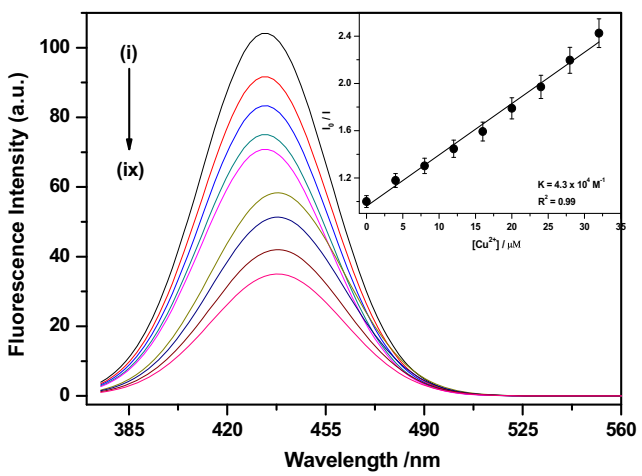

Fig. 5 Fluorescence emission spectra of $\mathbf{H_{11}L}$ in presence of different concentrations of Cu^{2+} in ethanol solution at room temperature. The concentrations of Cu^{2+} (μM) are: 0.0 (i), 4.0 (ii), 8.0 (iii), 12.0 (iv), 16.0 (v), 20.0 (vi), 24.0 (vii), 28.0 (viii) and 32.0 (ix). Inset shows the Stern-Volmer plot from titration of $\mathbf{H_{11}L}$ with different conc. of Cu^{2+} (0-32 μM)

with Cu^{2+} ion. The decrease in fluorescence emission intensity in our study may be due to strong metal-fluorophore communication compared to other interactions which leads to fluorescence quenching. So, the paramagnetic behavior of Cu^{2+} and the complex probe ($H_{11}L$-Cu^{2+}) interaction was the main reason for fluorescence quenching. The emission intensity of $\mathbf{H_{11}L}$ was linearly proportional to Cu^{2+} ion concentration. The detection limit was calculated and found to be in order of 10^{-5} M. Hence, $\mathbf{H_{11}L}$ shows selective estimation for Cu^{2+} and "turn-off" fluorescent sensor in presence of Cu^{2+} ion.

The fluorescence quenching behavior can be expressed mathematically by the Stern-Volmer relation [55] which allows calculating the quenching constant using Eq. (2).

$$\frac{I_0}{I} = 1 + K_{SV}[Q] \tag{2}$$

where, I_0 and I are fluorescence intensities in the absence and presence of quencher (Q), K_{sv} is the Stern-Volmer constant related to the bimolecular quenching rate constant and [Q] is the quencher concentration. This plot exhibits linear relationship indicating that $\mathbf{H_{11}L}$ is potentially useful for detection of Cu^{2+} with K_{sv} value of 4.3×10^4 M^{-1} (Fig. 5(inset)). To further investigate the quenching mechanism whether static or dynamic, we studied the change in absorption spectrum with an increase in Cu^{2+} ion concentration which clearly indicates the quenching mechanism to be static in nature. Moreover, we also monitored the fluorescence behavior in presence of ascorbic acid. Here, the fluorescence emission intensity increases drastically in presence of ascorbic acid (~30 μM) which indicates the masking of the quenching effect of copper.

Stoichiometry of Complexation

The stoichiometric ratio and apparent binding constant for ligand-metal ions complex was also determined by analyzing the changes in fluorescence emission intensity with different metal ions concentration. The apparent binding constant of the complex for 1:1 binding between ligand and metal ions can be obtained using modified form of Benesi-Hildebrand relation [56] written as

$$\frac{1}{F-F_0} = \frac{1}{F_\alpha - F_0} + \frac{1}{K(F_\alpha - F_0)} \times \frac{1}{[M^{2+}]} \tag{3}$$

where, F_0 and F are the fluorescence intensities in the absence and presence of metal ions respectively. F_α is the fluorescence intensity in the presence of excess amount of metal ions. Therefore, for 1:1 complex formation, the double reciprocal plot of $1/(F\text{-}F_0)$ against $1/[M^{2+}]$ should give a straight line; from the slope and intercept of which, the equilibrium constant (K) can be calculated. Figure 4(inset) shows the representative linear fitting using Eq. (3) and confirms 1:1 stoichiometry between $\mathbf{H_{11}L}$ and Zn^{2+} with association constant of 2.6×10^4 M^{-1}. At the same time, we also studied Job's plot analyses for determination of stoichiometry between $\mathbf{H_{11}L}$ and Zn^{2+}. The method is that keeping total concentration of $\mathbf{H_{11}L}$ and Zn^{2+} at 50.0 μM and changing the molar ratio of Zn^{2+} from 0.1 to 1.0. From Fig. 6(a) when molar fraction of Zn^{2+} was 0.5, the fluorescence emission maxima at 438 nm got to maximum, indicating that forming a 1:1 complex between $\mathbf{H_{11}L}$ and Zn^{2+}. Moreover, this further corroborated 1:1 complex formation based on B-H relationship. Similarly, in case of $\mathbf{H_{11}L}$ and Cu^{2+} complex formation, it was confirmed to be 1:1 stoichiometry between $\mathbf{H_{11}L}$ and Cu^{2+} with association constant of 8.6×10^4 M^{-1}. Figure 6(b) shows 1:1 complex formation between $\mathbf{H_{11}L}$ and Cu^{2+} based on Job's plot analyses.

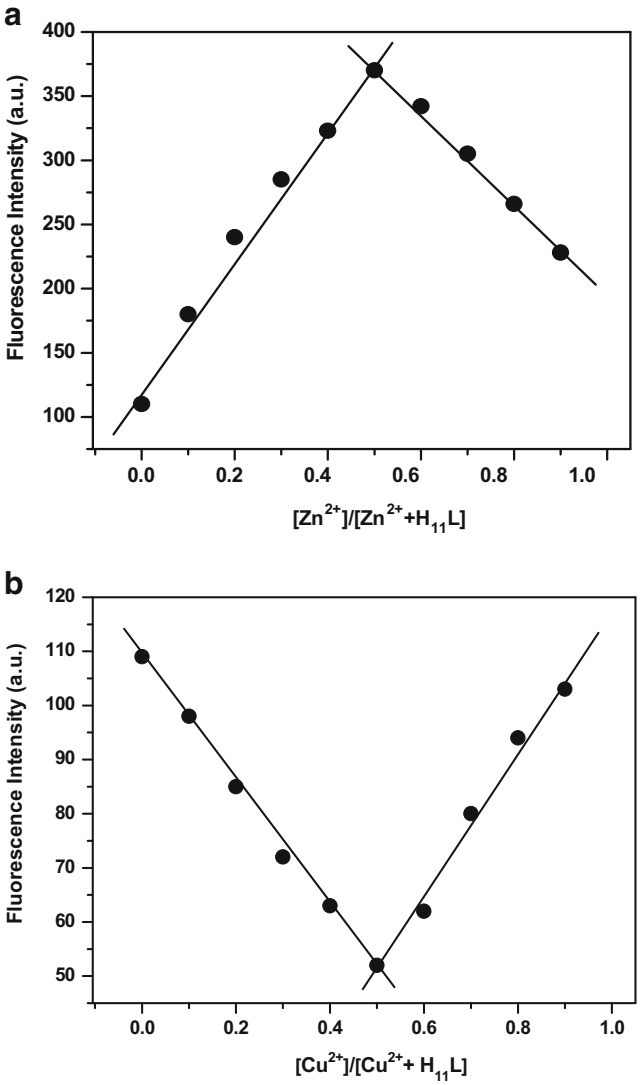

Fig. 6 Job's plot of **a** $H_{11}L$ (2.5×10^{-4} M) with Zn^{2+} ion and **b** $H_{11}L$ (2.5×10^{-4} M) with Cu^{2+} ion in ethanol solution at room temperature

We also determine the nature of binding ratio and binding sites of metal ions to $\mathbf{H_{11}L}$ using other form of B-H equation as given below.

$$\log\left((I-I_0)/(I_{max}-I)\right) = n\log[M^{2+}] - \log K_d \quad (4)$$

where I_0 and I are the fluorescence intensities in the absence and presence of metal ions respectively. I_{max} is the fluorescence intensity in presence of excess amount of metal ions. From the plot of $\log((I-I_0)/(I_{max}-I))$ versus $\log [M^{2+}]$ in Eq. (4), the slope and intercept were obtained giving the slope value, n = 1.28 indicating the binding ratio of Zn^{2+} ions to $\mathbf{H_{11}L}$ as 1:1 and $\log K_d$ was found to be 1.785. Similarly, in case of $\mathbf{H_{11}L}$ and Cu^{2+} complex formation, the slope and intercept were found to be slope value, n = 1.32 and $\log K_d$ = 1.62 indicating 1:1 binding nature of Cu^{2+} ions to $\mathbf{H_{11}L}$.

Effect of pH

We also studied the effect of pH both in presence and absence of Zn^{2+} and Cu^{2+} (Fig. 7). Over a wide range of pH, there was no obvious change in the fluorescence intensity of free ligand alone which clearly indicates insensitivity to pH. However, in presence of Zn^{2+}, $\mathbf{H_{11}L}$ has a strong pH dependent even though it had a weak fluorescence response to Zn^{2+} in acidic environment because of protonation of phenolic hydroxyl [57] leading to a weak coordination ability of Zn^{2+} [58]. However, satisfactory Zn^{2+} sensing abilities were exhibited with increasing pH. Thus, $\mathbf{H_{11}L}$ indicates a good fluorescence sensing ability to Zn^{2+} over a wide range from pH 5.5 to pH 11. Moreover, on addition of Cu^{2+}, quenching behavior was observed in the wide pH range from pH 4.0 to pH 11.5. These results also clearly indicate that $\mathbf{H_{11}L}$ can be employed as a selective fluorescent probe to recognize and distinguish Zn^{2+} and Cu^{2+} in presence of other survey metal ions.

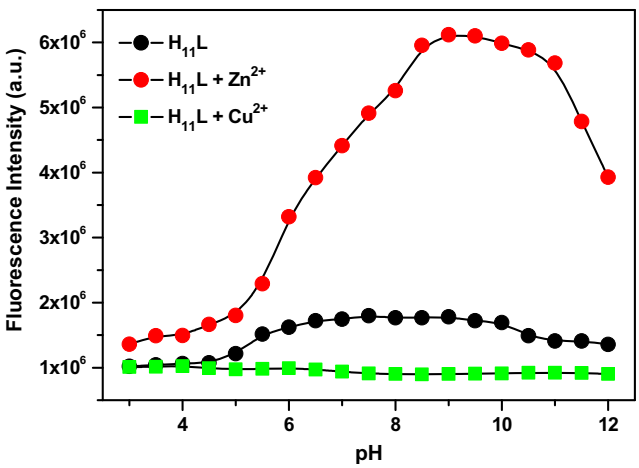

Fig. 7 Effect of pH on the fluorescence intensity of $H_{11}L$ (2.5×10^{-4} M) in absence (●) and presence (●) of Zn^{2+} ion and (■) of Cu^{2+} ion

Effect of Different Substituents

Metal-ligand complexes have been studied showing both the affect on the fluorescence emission wavelength and intensity of the ligand through metal coordination. The luminescent properties of Zn^{2+} complexes were reported to be determined by the organic ligand because of the electronic configuration of Zn^{2+} ($3d^{10}4s^0$) where the d-shell are completely filled which causes lack of intrinsic spectroscopic or magnetic signal [59]. Herein, the fluorescence behaviors of $\mathbf{H_{11}L}$ and complexes with different substituent of Zn^{2+} were studied in the solution phase at room temperature. Here, the emission spectra of complexes are very similar with $\mathbf{H_{11}L}$ except for the fluorescence intensity and peak position, indicating that the fluorescence of complexes is L-based emission. Meanwhile, the fluorescence emission for complexes were slightly blue-shifted compared to free ligand which is considered to mainly arise from the coordination of Zn^{2+} centre to $\mathbf{H_{11}L}$. The incorporation of Zn^{2+} effectively increases the conformational rigidity of the ligand and enhanced fluorescence intensities of all five complexes [60]. Moreover, the different in fluorescence intensities of the complexes with different substituent's like CO_3, SO_4, Cl, NO_3 and CH_3COO, can be explain due to bigger conformational rigidity for a 3D supramolecular network, as well as hydrogen bonds and π….π packing interactions [61].

Real Water Sample Assay

As we all know that zinc is the second most abundant and essential trace elements in the human body which play important roles in biology, chemistry and environment. Moreover, zinc is also a mineral that naturally occurs in rocks and soil and is a normal constituent of the human diet. So, in order to evaluate the application feasibility to determine Zn^{2+} ion in real water samples, several water samples from different water sources were selected including tap water, mineral water, river water, pond water, well water and distilled water. The changes in fluorescence emission intensity were measured after addition of 20% of the water samples to ethanol solution of the probe (Fig. 8). Here, the fluorescence intensity of the probe upon addition of 20% pond and well water indicates significant increase compared to other water samples, which indicates that the content of Zn^{2+} ion in pond and well water is high. However, in case of river and tap water, the fluorescence intensity is weak compared to pond and well water which indicates low content of Zn^{2+}. The possible reason might be due to low content of Zn^{2+} in river and tap water or due to the presence of different interfering metal ions compare to pond and well water. For mineral and distilled water, there is almost negligible enhancement of fluorescence intensity after addition of 20% of the water samples with suggests that the amount of Zn^{2+} ion in these two samples is very low.

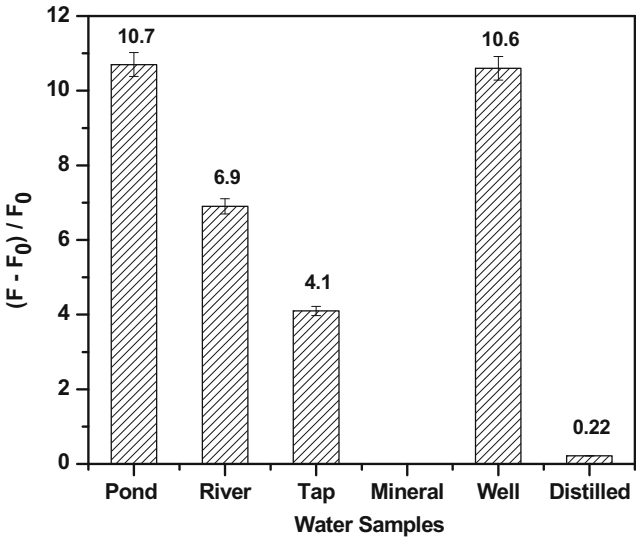

Fig. 8 Fluorescence intensity of ethanol solution of $\mathbf{H_{11}L}$ (2.5×10^{-4} M) with addition of 20% (%, *v*/v) water samples at room temperature

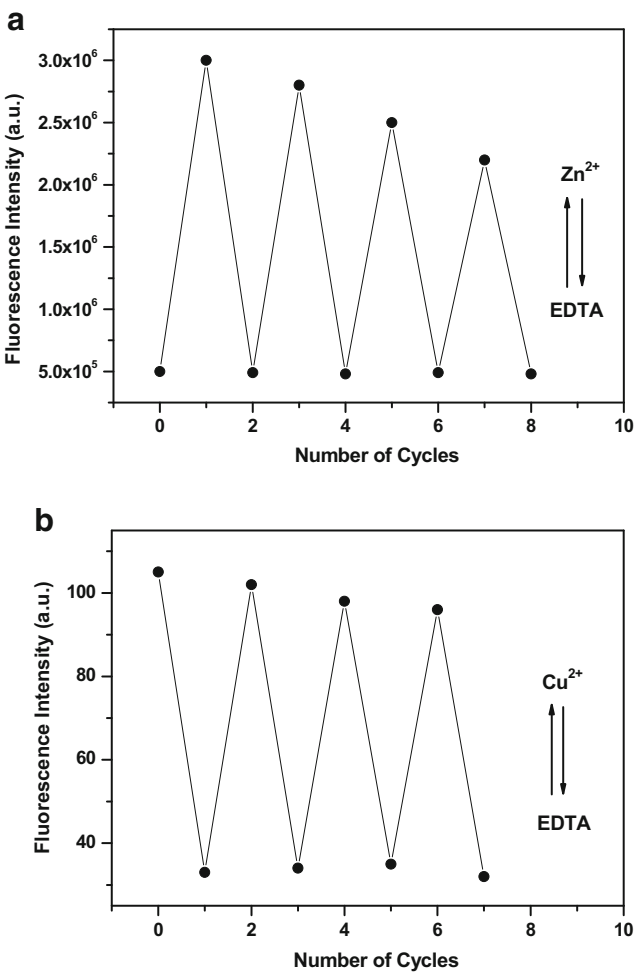

Fig. 9 Reversible changes in fluorescence intensity of $\mathbf{H_{11}L}$ at 484 nm after subsequent addition of **a** Zn^{2+} and EDTA and **b** Cu^{2+} and EDTA

Effect of EDTA

Reversibility nature of $\mathbf{H_{11}L}$ was also studied using EDTA as a coordinating ligand. Here, we have selected EDTA as a ligand of choice as it is available in abundance and relatively low cost. The fluorescence emission behavior of the complex probe ($H_{11}L$-Zn^{2+}) was monitored in presence of EDTA (~35 μM) and the fluorescence intensity was found to decrease and returned to lower level for $\mathbf{H_{11}L}$ indicating regeneration of free $\mathbf{H_{11}L}$ which became constant and corresponds to the fluorescent intensity of the free ligand. A similar type of reversibility nature for fluorescent sensor has already been reported earlier [62, 63]. This may be due to the lack of affinity of EDTA with $\mathbf{H_{11}L}$ as well as its ability to form a preferential complex with Zn^{2+} ions. Thus, using EDTA, free $\mathbf{H_{11}L}$ was regenerated from the complex probe ($H_{11}L$-Zn^{2+}) which can be reused for further Zn^{2+} sensing. Again on subsequent addition of Zn^{2+} and EDTA, the change in fluorescence emission intensity occurred reversibly even after several cycles (Fig. 9(a)). These results show that $\mathbf{H_{11}L}$ can be used as reversible fluorescent chemosensor using EDTA as coordinating ligand. Similarly, upon alternatively gradual addition of Cu^{2+} and EDTA, the change in fluorescence emission intensity shows reversibility to its original state up to several cycles as shown in fig. 9(b). Overall, these experiments confirm the reusability, recyclable and stability nature of the ligand, which may be used for wide practical applications.

Fluorescence Response Time in Presence of Zn^{2+} and Cu^{2+} Ions

The time dependent fluorescence intensity profiles of $\mathbf{H_{11}L}$ was performed in presence of three different concentrations of Zn^{2+} and Cu^{2+} ions, respectively. Figure 10(a) shows the fluorescence intensity profile curve showing instant enhancement in presence of Zn^{2+} ion with almost in no time. As the time increases, fluorescence intensity increases to a certain time ~ 30 s and remain almost unchanged over a period of time ~ 3 min, which may be due to strong complexation behavior of $\mathbf{H_{11}L}$ with Zn^{2+} ion via OH and N-heteroatoms due to photoinduced electron transfer. This performance also clearly indicates a good and much faster response compared to other available reports [64, 65] in addition of Zn^{2+} ion. However, in presence of Cu^{2+} ion, fluorescence intensity quenching behavior was observed in no time (Fig. 10(b)). Here, fluorescence intensity decreases to a certain time and remains constant over a period of time ~ 2 min. This decrease in fluorescence intensity may be due to strong metal-fluorophore communication which leads to fluorescence quenching. These experiments clearly indicates a good and short response time to monitor both Zn^{2+} and Cu^{2+} ions, respectively which can be further use for wide practical applications.

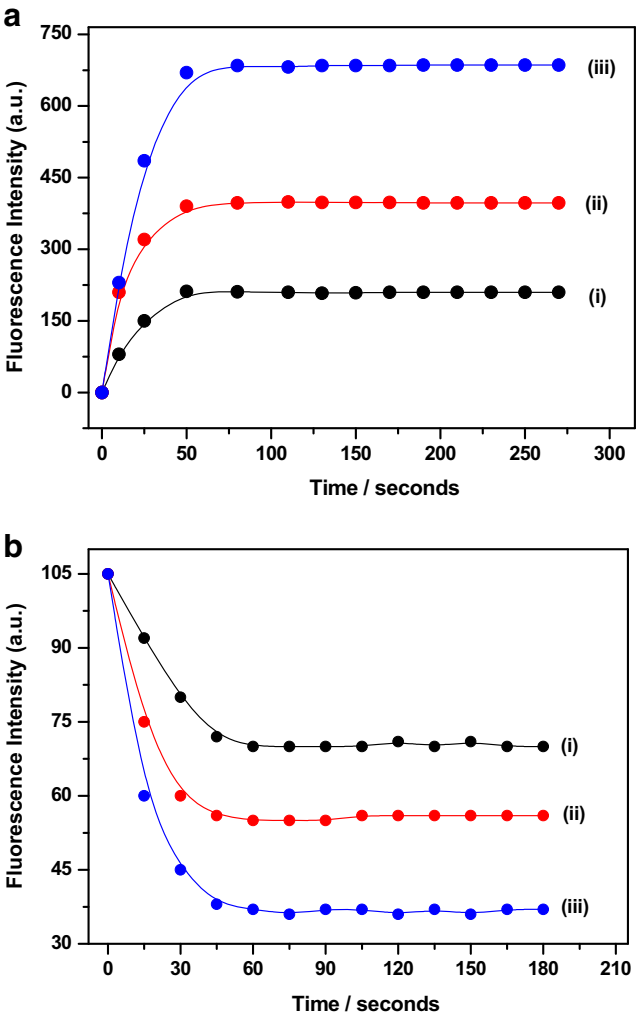

Fig. 10 Fluorescence response of $H_{11}L$ in presence of **a** Zn^{2+} with different concentrations at different times. The concentrations of Fe^{3+} (μM) are: (i) 10.0, (ii) 25.0 and (iii) 45.0, respectively. **b** Cu^{2+} with different concentrations at different times. The concentrations of Cu^{2+} (μM) are: (i) 10.0, (ii) 20.0 and (iii) 35.0, respectively

^{1}H NMR Titration and Mass Analysis

To understand the interaction and binding behavior of $\mathbf{H_{11}L}$ towards Zn^{2+} ion, ^{1}H NMR titration experiments were carried out in the absence and presence of different concentrations of Zn^{2+} ion in DMSO-d_6 solvent at room temperature. Here, four different NMR tubes containing $\mathbf{H_{11}L}$ dissolved in DMSO-d_6 were prepared and then three different concentrations (0.25 eq., 0.5 eq. and 1.0 eq of Zn^{2+} ions) of $Zn(CH_3COO)_2$ dissolved in DMSO-d_6 were also prepared and added to different NMR tubes. After shaking thoroughly for 1 min, ^{1}H NMR experiments were recorded at room temperature. As shown in the Fig. 11, the hydroxyl proton of $\mathbf{H_{11}L}$ obtained at around 10.16 ppm in the free ligand has experienced a remarkable downfield shift towards 10.52 ppm upon addition of Zn^{2+} ion. On the other hand, the aromatic protons signal at 8.57, 8.27, 7.84, 7.59, 7.29, 7.07, 6.18 ppm were shifted marginally downfield to 8.73, 8.62, 8.23, 8.04, 7.51, 7.74, 6.24 ppm while the other signals at 7.74, and 7.21 ppm were shifted marginally upfield to 7.16 and 6.97 ppm in presence of Zn^{2+} ion, respectively. These spectra exhibited the binding nature of $\mathbf{H_{11}L}$ with Zn^{2+} ion in 1:1 stiochiometric ratio [66]. Moreover, these overall changes in the chemical shifts of the proton in presence of Zn^{2+} ions suggested that the binding of $\mathbf{H_{11}L}$ to Zn^{2+} forms a rigid system by a strong complexation with $\mathbf{H_{11}L}$ via O-H and two N-atoms of pyridine and azomethine, respectively. These results also indicated the structural and conformational changes of $\mathbf{H_{11}L}$ upon Zn^{2+} ion binding. Again, ^{1}H NMR spectrum of the ligand was also recorded in different pH to confirm the stability of the ligand. Here, in this experiment, we have observed that the peak signals remain almost at same position throughout different pH which indicates insensitivity to pH.

To better understand the binding nature of $\mathbf{H_{11}L}$ with Zn^{2+} ion, ESI-mass spectra of $\mathbf{H_{11}L}$ and its complex ($H_{11}L$-Zn^{2+}) were also recorded and shown in Fig. 12. The observed molecular ion peak *m/z* for $\mathbf{H_{11}L}$ was obtained at 331.5. However, in presence of Zn^{2+} ion, the molecular ion peak *m/z* was found at 445.3 which correspond to [$H_{11}L$ + Zn^{2+}+ Acetate] $^+$ (calculated: 445.04). Here it is worth to mention that the complex ($H_{11}L$-Zn^{2+}) ensemble also involves a coordinated acetate molecule. So, these mass spectra also confirmed the binding nature of $\mathbf{H_{11}L}$ to Zn^{2+} as 1:1 stoichiometry [67].

Time-Resolved Fluorescence Measurements

Lifetime data of $\mathbf{H_{11}L}$ was obtained by nanosecond time-correlated single photon counting technique using 360 nm LED source and monitoring the emission at 428 nm. The fluorescence decay curves were analyzed by non-linear least-square iterative convolution method based on Lavenberg-Marquardt [68] chi-sqare (χ^2) minimization algorithm. Here, the fluorescence decay need two exponential function both for free ligand as well as the complex probe ($H_{11}L$-Zn^{2+}) to reproduce the experimental data points with acceptable statistical parameters like reduced chi-square (χ^2) values and Durbin-Watson parameter as demonstrated by visual inspection of the distribution of weighted residuals with time (Fig. 13). The biexponential fluorescence decay parameters for $\mathbf{H_{11}L}$: τ_1 = 0.63 ns (0.70) and τ_2 = 1.91 ns (0.30) and for $H_{11}L$-Zn^{2+}: τ_1 = 1.22 ns (0.29) and τ_2 = 3.66 ns (0.71), respectively. Here, it is seen that the amplitude of the short nanosecond component is much larger compared to long nanosecond component in free ligand. However, with addition of Zn^{2+}, the amplitude of the short nanosecond component is much smaller compared to long nanosecond component which may be due to suppression of PET process by metal ion binding. This complex nature of the fluorescence decay parameters is a reflection of the flexibility of the molecules

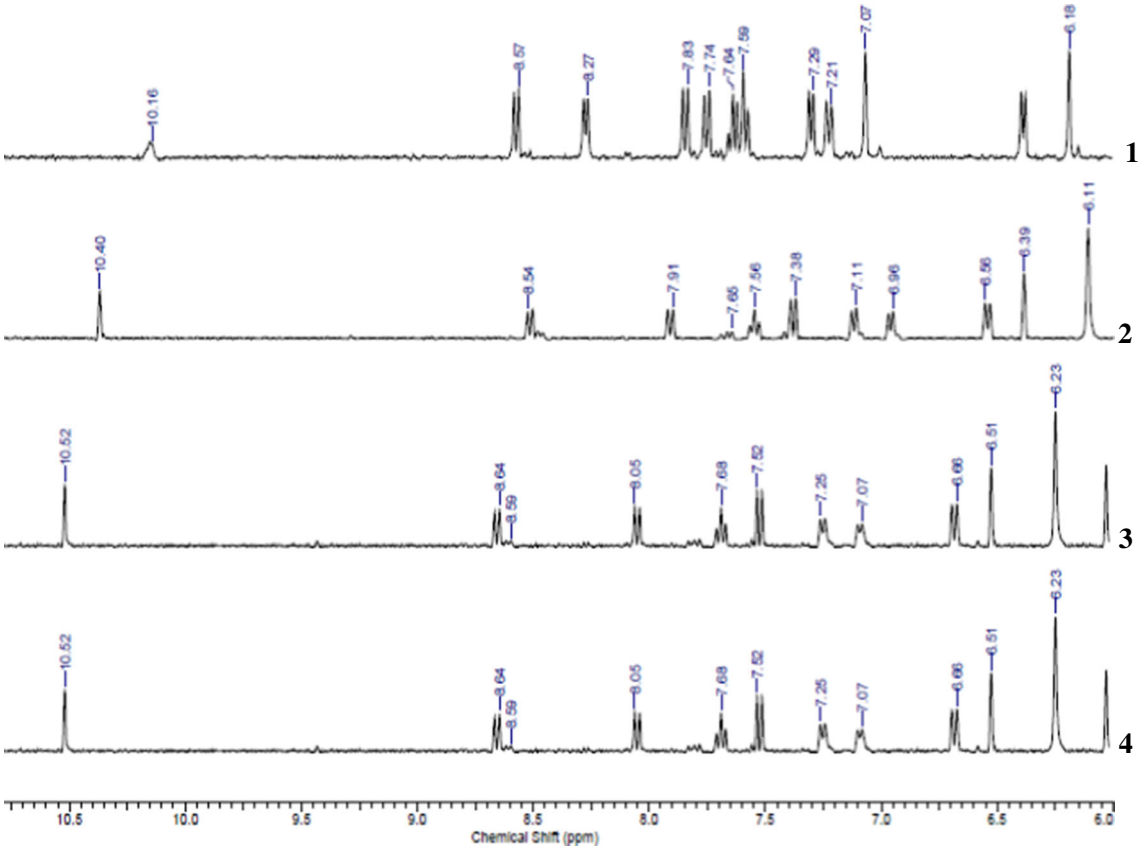

Fig. 11 ^{1}H NMR titration plot of $H_{11}L$ (1) with Zn^{2+} (2 = 0.25 eq., 3 = 0.50 eq. and 4 = 1.0 eq. of Zn^{2+}) ion in DMSO-d_6 solvent

[69]. Here, we calculate the average decay time of **$H_{11}L$** both in free ligand and complex probe using Eq. (5) to discuss the fluorescence decay behavior.

$$< \tau >= \sum_i \alpha_i \times \tau_i \quad (5)$$

The calculated average fluorescence decay values are 1.02 ns and 2.95 ns for free ligand and the complex probe ($H_{11}L$-Zn^{2+}), respectively. It is interesting to note that the average fluorescence decay time in ($H_{11}L$-Zn^{2+}) is about three times larger than the corresponding values in **$H_{11}L$**. So, the metal-ligand orbital mixing in the complex may be the reason for longer time passing in the excited state compared to free

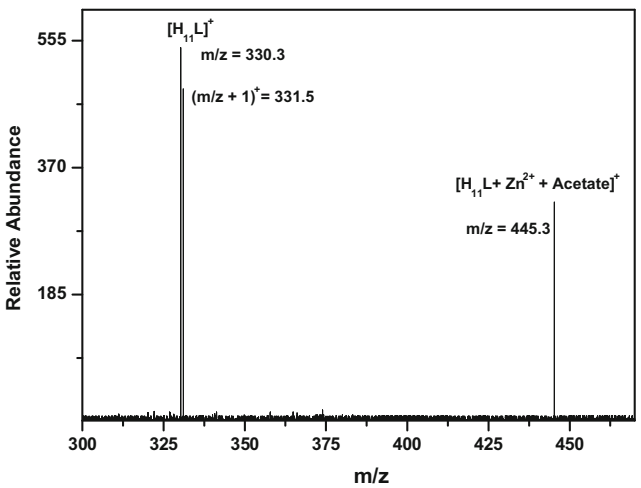

Fig. 12 ESI-MS spectra of $H_{11}L$ and its complex ($H_{11}L$-Zn^{2+})

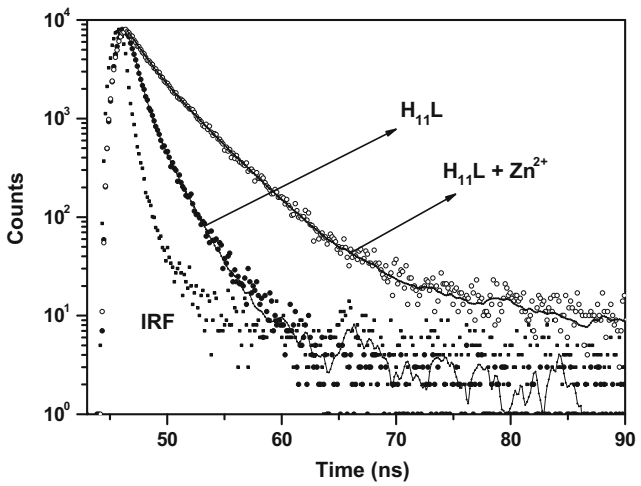

Fig. 13 Time-resolved fluorescence decay profile of **$H_{11}L$** in absence (free ligand) and presence of Zn^{2+}, respectively. IRF indicates instrument response function

Fig. 14 Truth table and the monomolecular circuit based on **a** Zn^{2+} and Cu^{2+} and **b** Zn^{2+} with EDTA and EDTA with Cu^{2+}. **a** Zn^{2+} and Cu^{2+}. **b** Zn^{2+} with EDTA and EDTA with Cu^{2+}

a

INPUT		OUTPUT
IN1	IN2	OUT
Zn^{2+}	Cu^{2+}	Emission at 428 nm
0	0	0
0	1	0
1	0	1
1	1	0

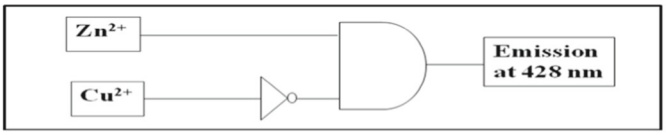

Zn^{2+} and Cu^{2+}

b

INPUT		OUTPUT
IN1	IN2	OUT
Zn^{2+}	EDTA	Emission at 428 nm
0	0	0
0	1	0
1	0	1
1	1	0
INPUT		OUTPUT
IN1	IN2	OUT
Cu^{2+}	EDTA	Emission at 428 nm
0	0	1
0	1	1
1	0	0
1	1	1

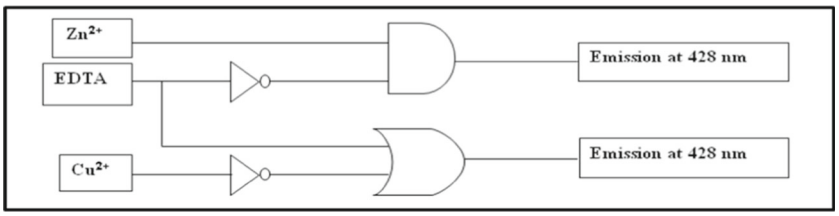

Zn^{2+} with EDTA and EDTA with Cu^{2+}

ligand. Here, we found that the fluorescence decay time was affected by turn-on sensor in presence of Zn^{2+}.

Application as Logic Function

The fluorescence emission behavior of $\mathbf{H_{11}L}$ can be utilized to study as a binary logic function with dual stimulating inputs as Zn^{2+} (IN1) and Cu^{2+} (IN2) and emission as output. With coordination of $\mathbf{H_{11}L}$ with Zn^{2+} (IN1) a new fluorescence emission band appears at 428 nm. Upon gradual addition of Cu^{2+} (IN2), the emission intensity of the band at 428 nm gets quenched. Herein, the coordination complex of $H_{11}L$-Zn^{2+} is replaced with Cu^{2+} due to greater abilities of binding with Cu^{2+} rather than Zn^{2+}. Actually it represents an AND gate with an inverter [70] in one of its input. Thus the emission change at 428 nm with Zn^{2+} as well as Cu^{2+} (with an inverter) as inputs can be interpreted as a monomolecular circuit showing an INHIBIT logic function [24–27]. Hence, the fluorescence behavior of $\mathbf{H_{11}L}$ can be applied for construction of INHIBIT logic function and its truth table (Fig. 14 (a)).

The regeneration of the free ligand was monitored with addition of EDTA as a good chelating agent. Here, the fluorescence emission intensity of the complex probe ($H_{11}L$-Zn^{2+}) returned to lower level for $\mathbf{H_{11}L}$ in presence of EDTA which corresponds to the fluorescence emission intensity of the free ligand. The decrease of fluorescence emission intensity and the emission band at 428 nm is almost disappeared indicating regeneration of free ligand. However in the absence of Zn^{2+}, EDTA does not have any effect on the emission intensity of $\mathbf{H_{11}L}$. Thus, with two chemical inputs as Zn^{2+} (IN1) and EDTA (IN2) and the emission as output, the molecular logic function was studied. Here, $\mathbf{H_{11}L}$ functions as an AND gate with an inverter in the EDTA input by monitoring the emission output. This function can be interpreted as a monomolecular circuit showing an INHIBIT logic function (Fig. 14(b)). As we know, upon addition of Cu^{2+}, the fluorescence

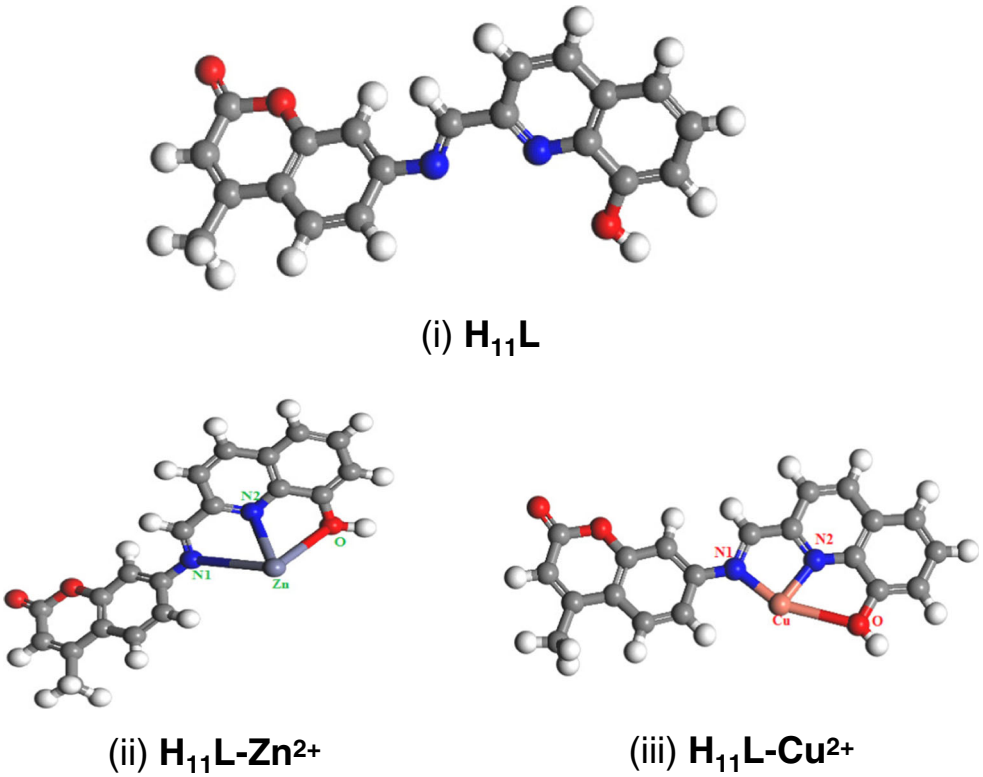

Fig. 15 DFT optimized structures of (i) $\mathbf{H_{11}L}$, (ii) $H_{11}L$-Zn^{2+} and (iii) $H_{11}L$-Cu^{2+} complexes evaluated at DNP/BLYP level

emission intensity band of $\mathbf{H_{11}L}$ at 428 nm gets quenched. However, with addition of EDTA as chelating agent to this complex ($H_{11}L$-Cu^{2+}), a pronounced fluorescence enhancement is observed which may be due to complex formation of EDTA with Cu^{2+} making the ligand free. So, in presence of EDTA to this complex, the fluorescence emission intensity is high compare only when Cu^{2+} is present alone. Thus, this behavior represents an OR gate with an inverter in one of its input which is also called an IMPLICATION logic gate [71–73] (Fig. 14 (b)).

Quantum Chemical Calculation

Initial structure of $\mathbf{H_{11}L}$ and its metal complexes ($H_{11}L$-Zn^{2+} and $H_{11}L$-Cu^{2+}) were both generated from the available experimental data in DFT calculations. The structure of $\mathbf{H_{11}L}$ and its metal complexes were fully optimized using BLYP functional and DNP basis sets as implemented in the program DMol^3 [44]. In order to confirm the stability of the complexes, we performed vibrational frequency calculations at the optimized structure with the same level of theory. The DFT

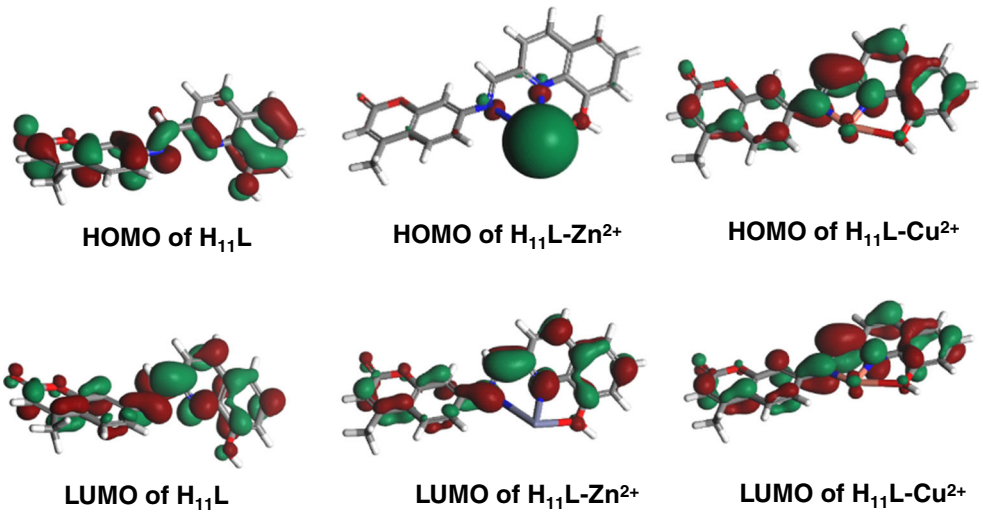

Fig. 16 DFT evaluated 3D isosurface HOMO and LUMO diagrams of $\mathbf{H_{11}L}$, $H_{11}L$-Zn^{2+} and $H_{11}L$-Cu^{2+} complexes, respectively

optimized geometries of **$H_{11}L$** and its metal complexes are shown in Fig. 15. In the vibrational frequency calculations, no imaginary frequency is observed for **$H_{11}L$** and its metal complexes which clearly suggest that the optimized compounds signify stable structures i.e., it shows local minima in the potential energy surfaces. It is observed from Fig. 15 that both zinc and copper metal centre are tri coordinated to the ligand through two nitrogen atoms and one OH group of ligand. It is noted from DFT generated data that selected bond lengths (Å) and bond angles (^{0}) for both Zn-complex and Cu-complex has been evaluated at B3LYP level. In Zn-complex, the bond length (Å) of Zn—N(1), Zn—N(2) and Zn—O are 2.698 Å, 2.452 Å and 3.021 Å, respectively. However, in case of Cu-complex, the bond length (Å) of Cu—N(1), Cu—N(2) and Cu—O are 1.983 Å, 1.981 Å and 2.783 Å, respectively. Here, metal-OH bond lengths in both complexes are longer than the other bond lengths. Moreover, the bond angles N(1)—Zn—N(2), N(1)—Zn—O and N(1)—Cu—N(2) and N(1)—Cu—O are found to be 61.224^0, 53.135^0, 89.072^0 and 70.325^0, respectively, around the metal atom. A distortion from 90^0 bond angle occurs for both $H_{11}L$-Zn^{2+} and $H_{11}L$-Cu^{2+} complexes, respectively. Here, $H_{11}L$-Zn^{2+} has more distorted compared to $H_{11}L$-Cu^{2+} as shown above which clearly indicates deviation from planar geometry.

The HOMO and LUMO energies of **$H_{11}L$** are calculated and found to be −5.211 eV and −3.018 eV, respectively. However, in case of metal complexes, the HOMO and LUMO are −5.018 eV and −3.184 eV for $H_{11}L$-Zn^{2+} as well as −3.829 eV and −3.657 eV for $H_{11}L$-Cu^{2+} complexes, respectively. The HOMO and LUMO isosurface diagrams of **$H_{11}L$** and its complexes ($H_{11}L$-Zn^{2+} and $H_{11}L$-Cu^{2+}) are shown in Fig. 16. The corresponding energy difference between HOMO-LUMO energy gap for **$H_{11}L$**, $H_{11}L$-Zn^{2+} and $H_{11}L$-Cu^{2+} are 2.193, 1.834 and 0.172 eV, respectively. Chemical hardness for both ligand as well as its metal complexes was also calculated. The chemical hardness value for **$H_{11}L$** is found to be 1.096 eV and that for its metal complexes are 0.917 eV and 0.086 eV for $H_{11}L$-Zn^{2+} and $H_{11}L$-Cu^{2+}, respectively. It is observed that Zn-complex has much higher stability compare to Cu-complex due to higher HOMO-LUMO energy gap as well as chemical hardness value.

Conclusions

In this work, we have designed and synthesized a new Schiff-base fluorescent probe -(E)-7-(((8-hydroxyquinolin-2-yl)methylene)amino)-4-methyl-2H-chromen-2-one (**$H_{11}L$**) which has been evaluated as a colorimetric sensor for Fe^{3+} and fluorescence "turn on-off" response for Zn^{2+} and Cu^{2+}. The UV-Vis absorption studies of **$H_{11}L$** indicate high selectivity for Fe^{3+} ion over other survey metal ions with a distinct color change, from colorless to deep yellow, which provide naked eye detection. Fluorescence studies of **$H_{11}L$** shows very high selectivity to Zn^{2+} and Cu^{2+} whereas other common alkali, alkaline earth and transition metal ions failed to induce response. The stoichiometric ratio and binding constant were evaluated using Benesi-Hildebrand relation giving 1:1 stoichiometry. This further corroborated 1:1 complex formation based on Job's plot analyses. These binding behaviors were also confirmed by ^{1}H NMR titration as well as ESI-Mass spectral analysis. This chemosensor exhibits a very good fluorescence sensing ability to Zn^{2+} over a wide pH range. An efficient way for the regeneration of free ligand from the complex probe was achieved using EDTA as a coordinating ligand which further can be reused for Zn^{2+} sensing. This chemosensor can be used as an important application for detection of Zn^{2+} in real water samples. **$H_{11}L$** exhibits two INHIBIT logic gates with two different chemical inputs (i) Zn^{2+} (IN1) and Cu^{2+} (IN2) and (ii) Zn^{2+} (IN1) and EDTA (IN2) and the emission as output. Again, an IMPLICATION logic gate is obtained with Cu^{2+} and EDTA as chemical inputs and emission as output mode. The corresponding energy difference between HOMO-LUMO energy gap for **$H_{11}L$**, $H_{11}L$-Zn^{2+} and $H_{11}L$-Cu^{2+} are 2.193, 1.834 and 0.172 eV, respectively. It is observed that Zn-complex has much higher stability compare to Cu-complex due to higher HOMO-LUMO energy gap as well as chemical hardness value. Moreover, this work provides an insight with a new approach for selective, sensitive and quantitative detection of these three most abundant and essential traces elements in the human body.

Acknowledgements Financial support through Start-Up Research Grant (Chemical Sciences) project No. SB/FT/CS-064/2012 from Science and Engineering Research Board (SERB), Government of India were gratefully acknowledged by Dr. T. Sanjoy Singh. The authors are indebted to Dr. S. itra and his research scholars for their help in TCSPC measurements. The authors are also highly acknowledged to CIF, IIT Guwahati for providing NMR and Mass spectra.

References

1. Silva APD, Gunaratne HQN, Gunnlaugsson T, Huxley AJM, McCoy CP, Rademacher JT, Rich TE (1997) Signaling recognition events with fluorescent sensors and switches. Chem Rev 97:1515–1566
2. Valeur B, Leray I (2000) Design principles of fluorescent molecular sensors for cation recognition. Coord Chem Rev 205:3–40
3. Lu Y, Berry SM, Pfister TD (2001) Engineering novel metalloproteins: design of metal-binding sites into native protein scaffolds. Chem Rev 101:3047–3080
4. Narayanaswamy S, Govindaraju T (2012) Aldazine-based colorimetric sensors for Cu^{2+} and Fe^{3+}. Sensors Actuators B Chem 161:304–310
5. Vallee BL, Falchuk KH (1993) The biochemical basis of zinc physiology. Physiol Rev 73:79–118
6. De Silva JJRF, Williams RJP (2001) The biological chemistry of elements: the inorganic chemistry of life, 2nd edn. Oxford University Press, New York

7. Bush AI, Pettingell WH, Multhaup G, Paradis M, Vonsattel JP, Gusella JF, Beyreuther K, Masters CL, Tanzi RE (1994) Rapid induction of Alzheimer a beta amyloid formation by zinc. Science 265:1464–1467
8. Koh JY, Suh SW, Gwag BJ, He YY, Hsu CY, Choi DW (1996) The role of zinc in selective neuronal death after transient global cerebral ischemia. Science 272:1013–1016
9. Walker CF, Black RE (2004) Zinc and the risk for infectious disease. Annu Rev Nutr 24:255–275
10. Danuta SK, Des RR (2005) The evolution of iron Chelators for the treatment of iron overload disease and cancer. Pharmacol Rev 579:547–583
11. Waggoner DJ, Bartnikas TB, Gitlin JD (1999) The role of copper in neurodegenerative disease. Neurobiol Dis 6:221–230
12. Vulpe C, Levinson B, Whitney S, Packman S, Gitschier J (1993) Isolation of a candidate gene for Menkes disease and evidence that it encodes a copper-transporting ATPase. Nat Genet 3:7–13
13. Bull PC, Thomas GR, Rommens JM, Forbes JR, Cox DW (1993) The Wilson disease gene is a putative copper transporting P-type ATPase similar to the Menkes gene. Nat Genet 5:327–337
14. Valentine JS, Hart PJ (2003) Misfolded Cu Zn SOD and amyotrophic lateral sclerosis. Proc Natl Acad Sci U S A 100:3617–3622
15. Bruijn LI, Miller TM, Cleveland DW (2004) Unraveling the mechanisms involved in motor neuron degeneration in ALS. Annu Rev Neurosci 27:723–749
16. Brown DR, Kozlowski H (2004) Biological inorganic and bioinorganic chemistry of neurodegeneration based on prion and Alzheimer diseases. Dalton Trans 13:1907–1917
17. De silva AP, Gunarane HQN, McCoy CP (1993) A molecular photoionic AND gate based on fluorescent signalling. Nature 364:42–44
18. Szacilowski K (2008) Digital information processing in molecular systems. Chem Rev 108:3481–3548
19. De Silva AP, McClenaghan ND (2004) Molecular-Scale Logic Gates. Chem Eur J 10:574–586
20. Pischel U (2007) Chemical approaches to molecular logic elements for addition and subtraction. Angew Chem Int Ed 46:4026–4040
21. Rurack K, Trieflinger C, Koval'chuck A, Daub J (2007) An Ionically driven molecular IMPLICATION gate operating in fluorescence mode. Chem Eur J 13:8998–9003
22. Zhao L, Sui D, Chai J, Wang Y, Jiang S (2006) Digital Logic Circuit Based on a Single Molecular System of Salicylidene Schiff Base. J Phys Chem B 110:24299–24304
23. Zhao L, Wang S, Wu Y, Hou Q, Wang Y, Jiang S (2007) Salicylidene Schiff Base assembled with Mesoporous silica SBA-15 as hybrid materials for molecular logic function. J Phys Chem C 111:18387–18391
24. Kaur N, Singh N, Caims D, Callan JF (2009) A Multifunctional Tripodal Fluorescent Probe: "Off–On" Detection of Sodium as well as Two-Input AND Molecular Logic Behavior. Org Lett 11:2229–2232
25. Kumar M, Dhir A, Bhalla V (2009) A molecular keypad lock based on the Thiacalix[4]arene of 1,3-alternate conformation. Org Lett 11: 2567–2570
26. Sarkar D, Pramanik A, Biswas S, Karmakar P, Mondol TK (2014) Al^{3+} selective coumarin based reversible chemosensor: application in living cell imaging and as integrated molecular logic gate. RSC Adv 4:30666–30672
27. Sarkar D, Pramanik A, Mondol TK (2015) A novel coumarin based molecular switch for dual sensing of Zn(II) and Cu(II). RSC Adv 5: 7647–7653
28. Suresh M, Das A (2009) New coumarin-based sensor molecule for magnesium and calcium ions. Tetrahedron Lett 50:5808–5812
29. Cao L, Jia C, Huang Y, Zhang Q, Wang N, Xue Y (2014) A highly selective fluorescence turn-on detection of Al^{3+} and Ca^{2+} based on a coumarin-modified rhodamine derivative. Tetrahedron Lett 55:4062–4066
30. El-Shekheby HA, Mangood AH, Hamza SM, Al-Kady AS, Ebeid EM (2014) A highly efficient and selective turn-on fluorescent sensor for Hg^{2+}, Ag^{+} and Ag nanoparticles based on a coumarin dithioate derivative. Luminescence 29:158–167
31. Hou J, Liu B, Li K, Yu K, Wu M, Yu X (2013) Two birds with one stone: Multifunctional and highly selective fluorescent probe for distinguishing Zn^{2+} from Cd^{2+} and selective recognition of sulfide anion. Talanta 116:434–440
32. Wang H, Feng Y, Meng S (2012) A novel fluorescent sensor for Fe^{3+} and Cr^{3+} based on a calix[4]arene bearing two coumarin units. J Chem Res 36:587–589
33. Wu J, Sheng R, Liu W, Wang P, Zhang H, Ma J (2012) Fluorescent sensors based on controllable conformational change for discrimination of Zn^{2+} over Cd^{2+}. Tetrahedron 68:5458–5463
34. Chattopadhyay N, Mallick A, Sengupta S (2006) Photophysical studies of 7-hydroxy-4-methyl-8-(4′-methylpiperazin-1′-yl) methylcoumarin: A new fluorescent chemosensor for zinc and nickel ions in water. J Photoch Photobio A 177:55–60
35. Liu A, Yang L, Zhang Z, Zhang Z, Xu D (2013) A novel rhodamine-based colorimetric and fluorescent sensor for the dual-channel detection of Cu^{2+} and Fe^{3+} in aqueous solutions. Dyes Pigments 99:472–479
36. Ang JQ, Nguyen BTT, Toh CS (2011) A dual K^{+}–Na^{+} selective Prussian blue nanotubes sensor. Sensors Actuators B Chem 157:417–423
37. Goswami S, Das S, Aich K, Sarkar D, Mondal TK (2013) Colorimetric as well as dual switching fluorescence 'turn on' chemosensors for exclusive recognition of Zn^{2+} and image in aqueous solution: experimental and theoretical studies. Tetrahedron Lett 54:6892–6896
38. Devaraj S, Tsui YK, Chiang CY, Yen YP (2012) A new dual functional sensor: highly selective colorimetric chemosensor for Fe^{3+} and fluorescent sensor for Mg^{2+}. Spectrochim Acta A 96:594–599
39. Beltrán OG, Cassels BK, Pérez C, Mena N, Núñez MT, Martínez NP (2014) Coumarin-based fluorescent probes for dual recognition of copper(II) and iron(III) ions and their application in bio-imaging. Sensors 14:1358–1371
40. Singh TS, Mitra S, Chandra AK, Tamai N, Kar S (2008) A combined experimental and theoretical study on photoinduced intramolecular charge transfer in trans-ethyl p-(dimethylamino)cinamate. J Photochem Photobiol A Chem 197:295–305
41. Becke AD (1988) Density-functional exchange-energy approximation with correct asymptotic behavior. Phys Rev A 38:3098–3100
42. Lee C, Yang W, Parr RG (1988) Development of the Colle-Salvetti correlation-energy formula into a functional of the electron density. Phys Rev B 37:785–789
43. Delly B, Ellis DE (1982) Efficient and accurate expansion methods for molecules in local density models. J Chem Phys 76:1949–1960
44. Delly B (1990) An all-electron numerical method for solving the local density functional for polyatomic molecules. J Chem Phys 92:508–517
45. Hohenberg P, Kohn W (1964) Inhomogeneous electron gas. Phys Rev 136(B):864–871
46. Kohn W, Sham L (1965) Self-consistent equations including exchange and correlation effects. Phys Rev 140:A1133–A1138
47. Moorthy S, Amal KM, Sukdeb S, Suresh E, Amit M, Rosa DL (2010) Azine-based receptor for recognition of Hg^{2+} ion: crystallographic evidence and imaging application in live cells. Org Lett 12: 5406–5409
48. Yin SC, Zhang J, Feng HK, Zhao ZJ, Xu LW, Qiu HY (2012) Zn^{2+}-selective fluorescent turn-on chemosensor based on terpyridine-substituted siloles. Dyes Pigments 95:174–179

49. Jayabharathi J, Thanikachalam V, Jayamoorthy K (2012) Effective fluorescent chemosensors for the detection of Zn^{2+} metal ion. Spectrochim Acta A 95:143–147
50. Reza A, Maisam P, Esmail T, Hassan K, Reza G (2011) Highly selective fluorescent recognition of Zn^{2+} based on naphthalene macrocyclic derivative. Spectrochim Acta A 82:200–204
51. Fegade U, Saini A, Sahoo SK, Singh N, Bendre R, Kuwar A (2014) 2,2′-(hydrazine-1,2-diylidenedimethylylidene)bis(6-isopropyl-3-methylphenol) based selective dual-channel chemosensor for Cu^{2+} in semi-aqueous media. RSC Adv 4:39639–39644
52. Wu QY, Anslyn EV (2004) Catalytic signal amplification using a heck reaction. An example in the fluorescence sensing of Cu(II). J Am Chem Soc 126:14682–14683
53. Zeng HH, Thompson RB, Maliwa BP, Fones GR, Moffet JW, Fierke CA (2003) Real-time determination of Picomolar free Cu(II) in seawater using a fluorescence-based fiber optic biosensor. Anal Chem 75:6807–6812
54. Hu J, Lü FT, Din LP, Zhang SJ, Fang Y (2007) A novel pyrene-based film: preparation, optical properties and sensitive detection of organic copper(II) salts. J Photochem Photobiol A 188:351–357
55. Lakowicz JR (2006) Principle of fluorescence spectroscopy. Plenum, New York
56. Benesi HA, Hildebrand JH (1949) A spectrophotometric investigation of the interaction of iodine with aromatic hydrocarbons. J Am Chem Soc 71:2703–2707
57. Roy P, Dhara K, Manassero M, Ratha J, Banerjee P (2007) Selective fluorescence zinc ion sensing and binding behavior of 4-methyl-2,6bis(((phenylmethyl)imino)methyl)phenol: biological application. Inorg Chem 46:6405–6412
58. Liu Y, Zhang N, Chen Y, Wang L (2007) Fluorescence sensing and binding behavior of Aminobenzenesulfonamidoquinolino-β-cyclodextrin to Zn^{2+}. Org Lett 9:315–318
59. Kotova OV, Eliseeva SV, Averjushkin AS, Lepnev LS, Vaschenko AA, Rogachev AY (2008) Zinc(II) complexes with Schiff bases derived from ethylenediamine and salicylaldehyde: the synthesis and photoluminescent properties. Russ Chem Bull Int Ed 57: 1880–1889
60. Majumder A, Rosair GM, Mallick A, Chattopadhyay N, Mitra S (2006) Synthesis, structures and fluorescence of nickel, zinc and cadmium complexes with the N,N,O-tridentate Schiff base N-2-pyridylmethylidene-2-hydroxy-phenylamine. Polyhedron 25: 1753–1762
61. Kang B, Weng L, Liu H, Wu D, Huang L, Lu C (1990) Syntheses, structures, and properties of vanadium, cobalt, and nickel compounds with 2-mercaptophenol. Inorg Chem 29:4873–4877
62. Gao C, Jin X, Yan X, An P, Zhang Y, Liu L (2013) A small molecular fluorescent sensor for highly selectivity of zinc ion. Sensors Actuators B Chem 176:775–781
63. Zhang D, Wang M, Chai M, Chen X, Ye Y, Zhao Y (2012) Label-free DNA sensor for detection of bladder cancer biomarkers in urine. Sensors Actuators B Chem 168:200–206
64. Thangaraj A, Gandhi S, Murugan I, Ayyanar S, Duraisamy C (2015) Aminobenzohydrazide based colorimetric and 'turn-on' fluorescence chemosensor for selective recognition of fluoride. Anal Chim Acta 876:1–8
65. Liu J, Meng X, Duan H, Xu T, Ding Z, Liu Y (2015) Two Schiff-base fluorescence probes based on triazole and benzotriazole for selective detection of Zn^{2+}. Sensors Actuators B 227:296–303
66. Gupta VK, Mergua N, Kumawata LK, Singh AK (2015) Selective naked-eye detection of magnesium (II) ions using a coumarin-derived fluorescent probe. Sensors Actuators B Chem 207:216–223
67. Kumar V, Kumar A, Diwan U, Shweta R, Srivastava SK (2015) Salicylideneimines as efficient dual channel emissive probes for Al3+: harnessing ESIPT and ICT processes. Sensors Actuators B Chem 207:650–657
68. Bevington PR (1969) Data reduction and error analysis for the physical sciences. McGraw-Hill Inc, New York
69. Sarkar M, Banthia S, Samanta A (2006) A highly selective 'off–on' fluorescence chemosensor for Cr(III). Tetrahedron Lett 47:7575–7578
70. López MV, Vázquez ME, Gómez Reino C, Pedrido R, Bermejo MR (2008) A metallo-supramolecular approach to a half-subtractor. New J Chem 32:1473–1477
71. Fu Y, Feng Q, Jiang X, Xu H, Li M, Zang S (2014) New fluorescent sensor for Cu^{2+} and S^{2-} in 100% aqueous solution based on displacement approach. Dalton Trans 43:5815–5822
72. Magri DC, Fava MC, Mallia CJ (2014) A sodium-enabled 'Pourbaix sensor': a three-input AND logic gate as a 'lab-on-a-molecule' for monitoring Na^{+}, pH and pE. Chem Commun 50: 1009–1011
73. Wang S, Men G, Zhao L, Hou Q, Jiang S (2010) Binaphthyl-derived salicylidene Schiff base for dual-channel sensing of Cu, Zn cations and integrated molecular logic gates. Sensors Actuators B Chem 145:826–831